Morphological Control of One-Dimensional Nanostructures of T-Shaped Asymmetric Bisphenazine

Kyoungmi Jang, John M. Kinyanjui, David W. Hatchett, and Dong-Chan Lee*

Department of Chemistry, University of Nevada Las Vegas, 4505 Maryland Parkway, Box 454003, Las Vegas, Nevada 89154-4003

Received October 28, 2008. Revised Manuscript Received April 2, 2009

This paper presents the morphological control of self-assembled structures derived from a novel T-shaped bisphenazine containing cyanophenyl groups. The π-aggregation of the molecule in solution was verified with ^{1}H NMR at various concentrations. Self-assembly using a phase transfer method showed morphological transformation from straight strands to flexible nanofibers with significant bundling and coiling, and finally, flat nanofibers with less bundling as solution concentration increased, which was extensively characterized by scanning electron microscopy (SEM). UV−vis spectroscopy in a binary solvent and solid state showed red-shifted absorption with increased absorbance at the long wavelength shoulder region when compared to that in the solution state. A variable temperature UV−vis experiment verified that the spectral change was caused by π-aggregation. X-ray diffraction (XRD) and Fourier-transform infrared (FT-IR) spectroscopy of the assembled structures showed that intermolecular cyano interactions are the major driving force for the formation of the nanofibers while $\pi-\pi$ interactions are dominant for the straight strands. The increased water contact angle (WCA) of nanofiber films in comparison to a spin-coated film is indicative of the nanoscale surface roughness and the hydrophobic nature of the nanofibers. This report provides a useful design tool based on the rational utilization of cyanophenyl groups in a large π-core to modulate assembly morphology.

Introduction

Self-assembly (SA) of π-conjugated materials through various intermolecular interactions has been a particularly useful bottom-up approach in preparing nanostructures with a high level of supramolecular organization. One-dimensionally (1D) grown nanostructures have drawn much attention for their potential applications in devices such as field effect transistors (FET)[1] and photovoltaics (PV)[2] because of their enhanced device performance. In addition, the ease of preparation of these nanostructures compared to single crystals offers an opportunity for facile device fabrications.[1,2b−d] The control of the morphology of self-assembled nanostructures from π-conjugated materials is of particular interest because many electro-optical properties including energy transfer and fluorescence modulation are influenced by the arrangement of π-cores.[3] Such a morphological control has been accomplished using strategic molecular design combined with a modulation of assembly conditions. A typical design approach has utilized the manipulation of side groups bonded to π-cores through the alteration of factors including the length,[4] branching,[5] and polarities.[6] Long and branched alkyl chains increase the solubility of large π-cores in common organic solvents which increases the processability by suppressing π-aggregation. However, selection of the types of side groups through sole consideration of solubility

* Corresponding author. E-mail: Dong-Chan.Lee@unlv.edu.

(1) (a) Xiao, S.; Tang, J.; Beetz, T.; Guo, X.; Tremblay, N.; Siegrist, T.; Zhu, Y.; Steigerwald, M.; Nuckolls, C. *J. Am. Chem. Soc.* **2006**, *128*, 10700–10701. (b) Briseno, A. L.; Roberts, M.; Ling, M.-M.; Moon, H.; Nemanick, E. J.; Bao, Z. *J. Am. Chem. Soc.* **2006**, *128*, 3880–3881. (c) Briseno, A. L.; Mannsfeld, S. C. B.; Lu, X.; Xiong, Y.; Jenekhe, S. A.; Bao, Z.; Xia, Y. *Nano Lett.* **2007**, *7*, 668–675. (d) Briseno, A. L.; Mannsfeld, S. C. B.; Reese, C.; Hancock, J. M.; Xiong, Y.; Jenekhe, S. A.; Bao, Z.; Xia, Y. *Nano Lett.* **2007**, *7*, 2847–2853.

(2) (a) Schmidt-Mende, L.; Fechtenkötter, A.; Müllen, K.; Moons, E.; Friend, R. H.; MacKenzie, J. D. *Science* **2001**, *293*, 1119–1122. (b) Yang, X.; Loos, J.; Veenstra, S. C.; Verhees, W. J. H.; Wienk, M. M.; Kroon, J. M.; Michels, M. A. J.; Janssen, R. A. J. *Nano Lett.* **2005**, *5*, 579–583. (c) Berson, S.; De Bettignies, R.; Bailly, S.; Guillerez, S. *Adv. Funct. Mater.* **2007**, *17*, 1377–1384. (d) Xin, H.; Kim, F. S.; Jenekhe, S. A. *J. Am. Chem. Soc.* **2008**, *130*, 5424–5425. (e) Wienk, M. M.; Turbiez, M.; Gilot, J.; Janssen, R. A. J. *Adv. Mater.* **2008**, *20*, 2556–2560.

(3) (a) Hoeben, F. J. M.; Jonkheijm, P.; Meijer, E. W.; Schenning, A. P. H. J. *Chem. Rev.* **2005**, *105*, 1491–1546. (b) Schenning, A. P. H. J.; Meijer, E. W. *Chem. Commun.* **2005**, 3245–3258. (c) Guerzo, A. D.; Olive, A. G. L.; Reichwagen, J.; Hopf, H.; Desvergne, J.-P. *J. Am. Chem. Soc.* **2005**, *127*, 17984–17985. (d) Ajayaghosh, A.; Praveen, V. K. *Acc. Chem. Res.* **2007**, *40*, 644–656. (e) Ajayaghosh, A.; Vijayakumar, C.; Praveen, V. K.; Babu, S. S.; Varghese, R. *J. Am. Chem. Soc.* **2006**, *128*, 7174–7175. (f) Ajayaghosh, A.; Praveen, V. K.; Vijayakumar, C. *Chem. Soc. Rev.* **2008**, *37*, 109–122.

(4) (a) Kim, J.-K.; Lee, E.; Huang, Z.; Lee, M. *J. Am. Chem. Soc.* **2006**, *128*, 14022–14023. (b) Lee, E.; Jeong, Y.-H.; Kim, J.-K.; Lee, M. *Macromolecules* **2007**, *40*, 8355–8360. (c) Yagai, S.; Kinoshita, T.; Higashi, M.; Kishikawa, K.; Nakanishi, T.; Karatsu, T.; Kitamura, A. *J. Am. Chem. Soc.* **2007**, *129*, 13277–13287.

(5) (a) Kastler, M.; Pisula, W.; Wasserfallen, D.; Pakula, T.; Müllen, K. *J. Am. Chem. Soc.* **2005**, *127*, 4286–4296. (b) Balakrishnan, K.; Datar, A.; Naddo, T.; Huang, J.; Oitker, R.; Yen, M.; Zhao, J.; Zang, L. *J. Am. Chem. Soc.* **2006**, *128*, 7390–7398.

(6) (a) Hill, J. P.; Jin, W.; Kosaka, A.; Fukushima, T.; Ichihara, H.; Shimomura, T.; Ito, K.; Hashizume, T.; Ishii, N.; Aida, T. *Science* **2004**, *304*, 1481–1483. (b) Yamamoto, Y.; Fukushima, T.; Suna, Y.; Ishii, N.; Saeki, A.; Seki, S.; Tagawa, S.; Taniguchi, M.; Kawai, T.; Aida, T. *Science* **2006**, *314*, 1761–1764. (c) Kim, J.-K.; Lee, E.; Lee, M. *Angew. Chem., Int. Ed.* **2006**, *45*, 7195–7198. (d) Che, Y.; Datar, A.; Balakrishnan, K.; Zang, L. *J. Am. Chem. Soc.* **2007**, *129*, 7234–7235. (e) Feng, X.; Pisula, W.; Zhi, L.; Takase, M.; Müllen, K. *Angew. Chem., Int. Ed.* **2008**, *47*, 1703–1706.

10.1021/cm8029455 CCC: $40.75
Published on Web 05/01/2009

often hampers effective π-aggregation and fails to produce well-assembled structures. Secondary interactions such as hydrogen bonding,[4c,7] dipole−dipole interaction,[6e,7u,8] amphiphilic interaction,[4a,b,6a−d] etc., in conjunction with $\pi-\pi$ interaction have also been used to control the morphologies of self-assembled structures. These interactions either compete or cooperate with $\pi-\pi$ interaction, which leads to the variation of the assembled morphologies. Among the various secondary interactions, classical hydrogen bonding has been a common choice to aid $\pi-\pi$ interaction by geometric cooperation with limited morphology control because of its high rigidity and spatial orientation. In contrast, weak intermolecular interactions such as dipole−dipole interaction and nonclassical hydrogen bonding between polar atoms and aromatic protons are rarely studied for the purpose of SA. However, weak interactions can assist $\pi-\pi$ stacking and control the morphologies by changing assembly conditions such as assembly method, solvent polarity, and concentrations.[9] For example, in the 1D SA from [2-(*p*-dimethylaminophenyl)ethenyl]-pheyl-methylene-propanedinitrile (DAPMP), an intramolecular charge transfer compound with two distinct directions of dipole moment showed controllable nanostructures depending on assembly temperature, which can control the direction of dipole resulting in different molecular arrangement.[8c] Therefore, the introduction of weak interactions could be an effective strategy for morphology control because those interactions are very responsive to external assembly conditions.

The cyano moiety has been an attractive functional group among other polar groups because of its 2-fold utility. It can be used to generate *n*-type semiconductors because of its strong electron-withdrawing nature,[10] and it has the ability to interact with either other cyano groups[11] or other atoms such as halogen,[12] sulfur in thiophenes,[10h] and hydrogen in aromatic rings.[10c,13] Although the former utility has been extensively studied, most of the latter utility has been narrowly focused on either strengthening molecular packing in crystal form[10c,h,11−13] or assembly behavior at the solid−vacuum interface.[14] In a surface-based assembly of cyanophenyl substituted porphyrins using ultra high-vacuum deposition, it has been demonstrated that the molecular arrangements such as dimer, trimer, tetramer, or linear chain can be induced by altering the position of the cyanophenyl group. For example, when two cyanophenyl groups are substituted at the trans position of the porphyrin, linear chain propagation on a Au substrate surface was observed because of hydrogen-binding interactions between cyanophenyl substituents.[14a,e] Despite such applications of cyano interaction, only a few examples[15] are related to solution-based 1D SA inducing free-standing nanostructures through cyano interaction.

A sensible molecular design can take advantage of all of the properties afforded by the cyano group to generate 1D nanostructures of *n*-type semiconductors with controllable assembly morphologies. We recently reported the initial SA behavior of a novel T-shaped asymmetric bisphenazine

(7) (a) Kimizuka, N.; Kawasaki, T.; Hirata, K.; Kunitake, T. *J. Am. Chem. Soc.* **1995**, *117*, 6360–6361. (b) Würthner, F.; Thalacker, C.; Sautter, A. *Adv. Mater.* **1999**, *11*, 754–758. (c) Ajayaghosh, A.; George, S. J. *J. Am. Chem. Soc.* **2001**, *123*, 5148–5149. (d) Shu, W.; Valiyaveettil, S. *Chem. Commun.* **2002**, 1350–1351. (e) van Gorp, J. J.; Vekemans, J. A. J. M.; Meijer, E. W. *J. Am. Chem. Soc.* **2002**, *124*, 14759–14769. (f) Jonkheijm, P.; Hoeben, F. J. M.; Kleppinger, R.; van Herrikhuyzen, J.; Schenning, A. P. H. J.; Meijer, E. W. *J. Am. Chem. Soc.* **2003**, *125*, 15941–15949. (g) Ajayaghosh, A.; George, S. J.; Praveen, V. K. *Angew. Chem., Int. Ed.* **2003**, *42*, 332–335. (h) Jonkheijm, P.; Miura, A.; Zdanowska, M.; Hoeben, F. J. M.; De Feyter, S.; Schenning, A. P. H. J.; De Schryver, F. C.; Meijer, E. W. *Angew. Chem., Int. Ed.* **2004**, *43*, 74–78. (i) George, S. J.; Ajayaghosh, A.; Jonkheijm, P.; Schenning, A. P. H. J.; Meijer, E. W. *Angew. Chem., Int. Ed.* **2004**, *43*, 3422–3425. (j) Varghese, R.; George, S. J.; Ajayaghosh, A. *Chem. Commun.* **2005**, 593–595. (k) George, S. J.; Ajayaghosh, A. *Chem.−Eur. J.* **2005**, *11*, 3217–3227. (l) Li, X.-Q.; Stepanenko, V.; Chen, Z.; Prins, P.; Siebbeles, L. D. A.; Würthner, F. *Chem. Commun.* **2006**, 3871–3873. (m) Ajayaghosh, A.; Varghese, R.; George, S. J.; Vijayakumar, C. *Angew. Chem., Int. Ed.* **2006**, *45*, 1141–1144. (n) Ajayaghosh, A.; Varghese, R.; Praveen, V. K.; Mahesh, S. *Angew. Chem., Int. Ed.* **2006**, *45*, 3261–3264. (o) Ajayaghosh, A.; Varghese, R.; Mahesh, S.; Praveen, V. K. *Angew. Chem., Int. Ed.* **2006**, *45*, 7729–7732. (p) Praveen, V. K.; George, S. J.; Varghese, R.; Vijayakumar, C.; Ajayaghosh, A. *J. Am. Chem. Soc.* **2006**, *128*, 7542–7550. (q) Ajayaghosh, A.; Praveen, V. K.; Vijayakumar, C.; George, S. J. *Angew. Chem., Int. Ed.* **2007**, *46*, 6260–6265. (r) Jancy, B.; Asha, S. K. *Chem. Mater.* **2008**, *20*, 169–181. (s) Yagai, S.; Seki, T.; Karatsu, T.; Kitamura, A.; Würthner, F. *Angew. Chem., Int. Ed.* **2008**, *47*, 3367–3371. (t) Yagai, S.; Mahesh, S.; Kikkawa, Y.; Unoike, K.; Karatsu, T.; Kitamura, A.; Ajayaghosh, A. *Angew. Chem., Int. Ed.* **2008**, *47*, 4691–4694. (u) Jordan, B. J.; Ofir, Y.; Patra, D.; Caldwell, S. T.; Kenneday, A.; Joubanian, S.; Rabani, G.; Cooke, G.; Rotello, V. M. *Small* **2008**, *4*, 2074–2078.

(8) (a) Mamiya, J.; Kanie, K.; Hiyama, T.; Ikeda, T.; Kato, T. *Chem. Commun.* **2002**, 1870–1871. (b) Miao, Q.; Lefenfeld, M.; Nguyen, T.-Q.; Siegrist, T.; Kloc, C.; Nuckolls, C. *Adv. Mater.* **2005**, *17*, 407–412. (c) Zhang, X.; Zhang, X.; Zou, K.; Lee, C.-S.; Lee, S.-T. *J. Am. Chem. Soc.* **2007**, *129*, 3527–3532. (d) Ajayaghosh, A.; Praveen, V. K.; Srinivasan, S.; Varghese, R. *Adv. Mater.* **2007**, *19*, 411–415. (e) Isoda, K.; Yasuda, T.; Kato, T. *J. Mater. Chem.* **2008**, *18*, 4522–4528.

(9) (a) Zhu, G.; Dordick, J. S. *Chem. Mater.* **2006**, *18*, 5988–5995. (b) Cai, W.; Wang, G.-T.; Xu, Y.-X.; Jiang, X.-K.; Li, Z.-T. *J. Am. Chem. Soc.* **2008**, *130*, 6936–6937. (c) Jiang, L.; Fu, Y.; Li, H.; Hu, W. *J. Am. Chem. Soc.* **2008**, *130*, 3937–3941.

(10) (a) Greenham, N. C.; Moratti, S. C.; Bradley, D. D. C.; Friend, R. H.; Holmes, A. B. *Nature (London)* **1993**, *365*, 628–630. (b) Halls, J. J. M.; Walsh, C. A.; Greenham, N. C.; Marseglia, E. A.; Friend, R. H.; Moratti, S. C.; Holmes, A. B. *Nature (London)* **1995**, *376*, 498–500. (c) Barclay, T. M.; Cordes, A. W.; MacKinnon, C. D.; Oakley, R. T.; Reed, R. W. *Chem. Mater.* **1997**, *9*, 981–990. (d) Granström, M.; Petritsch, K.; Arias, A. C.; Lux, A.; Andersson, M. R.; Friend, R. H. *Nature (London)* **1998**, *395*, 257–260. (e) Bader, M. M.; Custelcean, R.; Ward, M. D. *Chem. Mater.* **2003**, *15*, 616–618. (f) Jones, B. A.; Ahrens, M. J.; Yoon, M.-H.; Facchetti, A.; Marks, T. J.; Wasielewski, M. R. *Angew. Chem., Int. Ed.* **2004**, *43*, 6363–6366. (g) Jones, B. A.; Facchetti, A.; Marks, T. J.; Wasielewski, M. R. *Chem. Mater.* **2007**, *19*, 2703–2705. (h) Pappenfus, T. M.; Hermanson, B. J.; Helland, T. J.; Lee, G. G. W.; Drew, S. M.; Mann, K. R.; McGee, K. A.; Rasmussen, S. C. *Org. Lett.* **2008**, *10*, 1553–1556.

(11) (a) Manisekaran, T.; Bamezai, R. K.; Sharma, N. J.; Prasad, J. S. *Mol. Cryst. Liq. Cryst.* **1995**, *268*, 83–87. (b) Kuribayashi, M.; Hori, K. *Liq. Cryst.* **1999**, *26*, 809–815.

(12) (a) Reddy, D. S.; Panneerselvam, K.; Pilati, T.; Desiraju, G. R. *J. Chem. Soc. Chem. Commun.* **1993**, 661–662. (b) Reddy, D. S.; Ovchinnikov, Y. E.; Shishkin, O. V.; Struchkov, Y. T.; Desiraju, G. R. *J. Am. Chem. Soc.* **1996**, *118*, 4085–4089.

(13) (a) Manisekaran, T.; Bamezai, R. K.; Sharma, N. K.; Prasad, J. S. *Mol. Cryst. Liq. Cryst.* **1995**, *268*, 45–50. (b) Manisekaran, T.; Bamezai, R. K.; Sharma, N. K.; Prasad, J. S. *Liq. Cryst.* **1997**, *23*, 597–601. (c) Nishida, J.; Naraso; Murai, S.; Fujiwara, E.; Tada, H.; Tomura, M.; Yamashita, Y. *Org. Lett.* **2004**, *6*, 2007–2010.

(14) (a) Yokoyama, T.; Yokoyama, S.; Kamikado, T.; Okuno, Y.; Mashiko, S. *Nature (London)* **2001**, *413*, 619–621. (b) Bonifazi, D.; Spillmann, H.; Kiebele, A.; de Wild, M.; Seiler, P.; Cheng, F.; Güntherodt, H.-J.; Jung, T.; Diederich, F. *Angew. Chem., Int. Ed.* **2004**, *43*, 4759–4763. (c) Spillmann, H.; Kiebele, A.; Stöhr, M.; Jung, T. A.; Bonifazi, D.; Cheng, F.; Diederich, F. *Adv. Mater.* **2006**, *18*, 275–279. (d) Wintjes, N.; Bonifazi, D.; Cheng, F.; Kiebele, A.; Stöhr, M.; Jung, T.; Spillmann, H.; Diederich, F. *Angew. Chem., Int. Ed.* **2007**, *46*, 4089–4092. (e) Wintjes, N.; Hornung, J.; Lobo-Checa, J.; Voigt, T.; Samuely, T.; Thilgen, C.; Stöhr, M.; Diederich, F.; Jung, T. A. *Chem.−Eur. J.* **2008**, *14*, 5794–5802.

(15) Lim, G. S.; Jung, B. M.; Lee, S. J.; Song, H. H.; Kim, C.; Chang, J. Y. *Chem. Mater.* **2007**, *19*, 460–467.

containing cyano groups which were introduced to increase electron-affinity.[16] T-shaped aromatic cores are interesting π-platforms for SA, especially when they are functionalized with proper side groups as demonstrated previously.[17] With the T-shaped bisphenazine system, we found a dramatic morphological change from rigid microstrands to flexible nanofibers by the introduction of the cyano group to the same T-π-core, indicating that the morphological change was presumably induced by intermolecular cyano interaction. This result has inspired us to investigate the SA of the compound **1** under various assembly conditions to control morphology through the competition between $\pi-\pi$ interaction and cyano interaction. In this paper, we present a detailed spectroscopic investigation of the morphological transformation of the self-assembled structures as a function of the assembly conditions with various instrumental analyses. To the best of our knowledge, this work is the first example of such a study.

Experimental Section

Characterizations. ^{1}H NMR spectra were measured using a Varian Gemini 400 MHz NMR spectrometer at room temperature. Deuterated chloroform ($CDCl_3$) containing TMS as intrareference was used as the solvent for concentration-dependent ^{1}H NMR study. Absorption spectra were obtained with a Shimadzu UV-2450 UV−visible spectrometer in solution and solid state. SEM images were obtained by JSM-5600, JEOL SEM operating at 15 kV. The assembled structures obtained from different concentration solutions were transferred onto a gold/mica substrate, followed by air drying. The dried samples were coated with gold prior to SEM imaging. XRD powder patterns were collected on a Pananalytical X'Pert PRO X-ray diffractometer, for which a Cu Kα radiation (λ = 1.54 Å, 40 mA, 40 mV) was used. The sample was drop cast in a zero background plate for analysis. FT-IR measurement for a solution of **1** was performed using an IRPrestige-21 Shimadzu spectrometer. A solution of 1.8×10^{-5} M in CCl_4 was measured in a KBr cell with 1 mm spacing at room temperature. All FT-IR measurements for solid samples were performed using a Varian FTS-7000 spectrometer using attenuated total reflectance (ATR) crystal (Ge) and single point absorption micro reflectance FT-IR microscopy. A total of 500 scans at a 4 cm^{-1} resolution were collected for each sample. The assembled structures obtained from different concentration solutions were dispersed on a glass slide prior to ATR and absorption reflectance FT-IR measurements. The measurement of WCA was carried out using a contact angle goniometer (Dataphysics OCA15) at room temperature. A droplet of water (5 μL) was placed on surface coated with compound **1** and WCA was measured after 30 s. The average WCA was obtained by the measurement at ten different positions of each sample.

Recrystallization. A methylene chloride solution (2 mL) of **1** (25 mg, 0.02 mmol) was prepared, followed by standing without disturbing for a few days to grow crystals upon a slow evaporation of the solvent, which initially formed after 24 h.

Self-Assembly. SA of **1** was performed through a phase transfer method with a methylene chloride/methanol binary solvent system. Methylene chloride solutions (5 mL) of **1** with various concentrations (between 0.1 and 8 mM) were prepared in a 20 mL vial. Then, 4 mL of methanol was slowly added to the vial so that two phases were maintained. The mixture was left undisturbed at room temperature for 12 h to induce SA.

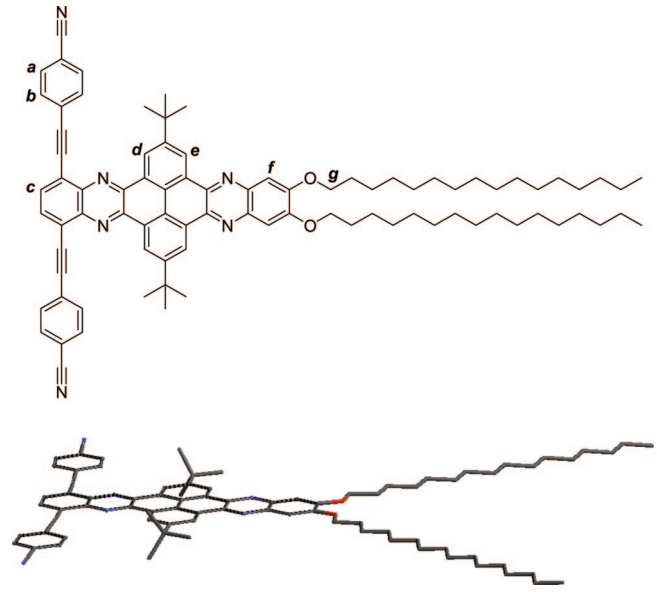

Figure 1. Molecular structure of **1** (top) and optimized geometry by B3LYP/6-31G* calculations (bottom; hydrogen atoms were omitted for clarity).

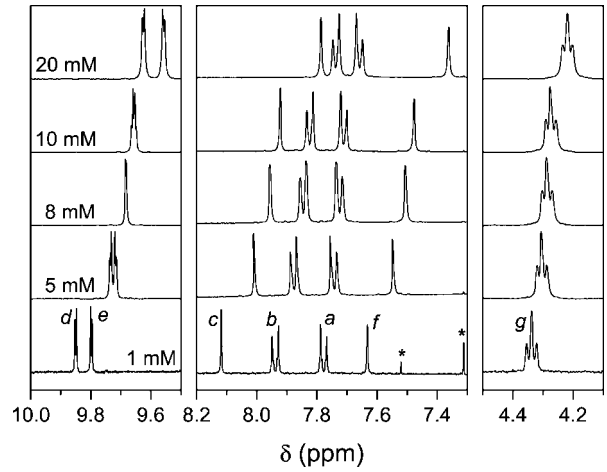

Figure 2. Concentration-dependent ^{1}H NMR spectra of **1** in $CDCl_3$.

Results and Discussion

The T-π-core in compound **1** adapts a planar geometry, with cyano groups being placed in the same plane as the T-core according to the theoretical calculation (Figure 1). This indicates that the planar structure of the molecule can stimulate effective intermolecular π-orbital overlap.

The molecular aggregation behavior of compound **1** was studied using ^{1}H NMR spectroscopy as a function of the concentration (Figure 2). For the peak assignments, the NMR spectrum of the 1 mM solution was used. The doublets at δ = 9.85 and 9.80 were assigned to H_d and H_e, respectively, whereas singlets at δ = 8.12 and 7.63 were assigned to H_c and H_f in the bisphenazine unit, respectively. The protons H_a and H_b in the cyanophenyl showed doublet peaks at δ = 7.78 and 7.94. The four aliphatic protons (H_g) in the alkoxy side groups were observed at δ = 4.34 as a triplet. As the concentration was increased from 1 to 20 mM, the

(16) Lee, D.-C.; Jang, K.; McGrath, K. K.; Uy, R.; Robins, K. A.; Hatchett, D. W. *Chem. Mater.* **2008**, *20*, 3688–3695.
(17) Moon, K.-S.; Kim, H.-J.; Lee, E.; Lee, M. *Angew. Chem., Int. Ed.* **2007**, *46*, 6807–6810.

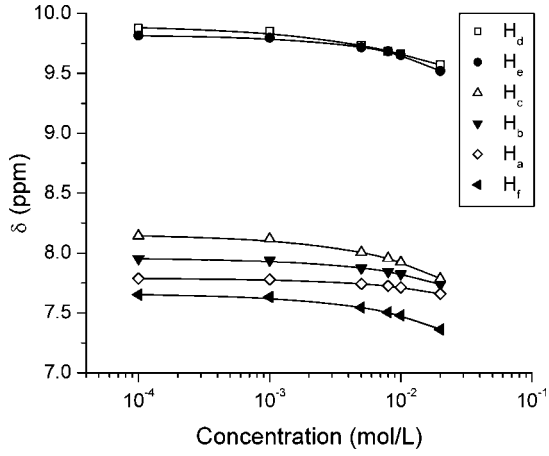

Figure 3. Concentration-dependent ^{1}H NMR data of **1** in $CDCl_3$ (symbols), fitted with the dimerization model (solid lines).

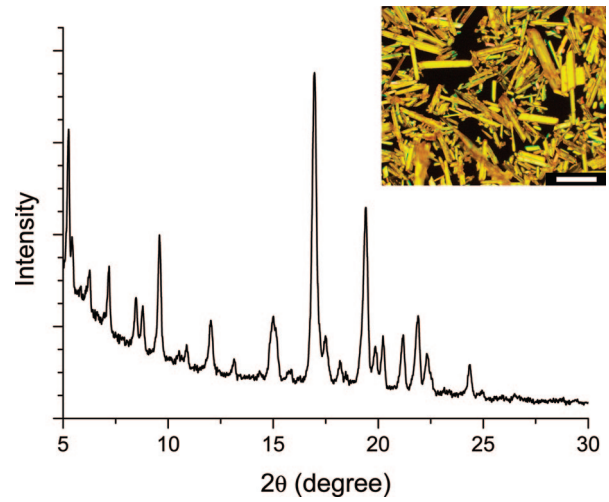

Figure 4. X-ray diffraction patterns of crystal of **1** obtained from 10 mM methylene chloride solution. Inset represents polarized optical micrograph (scale bar: 100 μm).

chemical shifts of all aromatic protons showed upfield shift by a range of 0.12−0.33 ppm. Among them, H_d and H_e showed an interesting trend. From 1 to 8 mM, H_d showed a larger upfield shift than H_e, merging to be a singlet at $\delta = 9.68$ at 8 mM. At concentrations higher than 8 mM, the splitting pattern of those two protons resumed. In addition, from 8 to 20 mM, H_e showed a larger upfield shift than H_d. This interesting observation suggests that H_d experiences more π-shielding than H_e at concentrations up to 8 mM, and vice versa beyond 8 mM. In the case of aliphatic protons, only H_g showed a slight upfield shift as the solution concentration increased. The upfield shift of all aromatic protons and the aliphatic protons nearby the aromatic core is due to the shielding effects of the aromatic ring above the respective protons and indicative intermolecular $\pi-\pi$ interaction. It should be noted that peak broadening was observed as the concentration increased because of restricted molecular motion. The most pronounced shift ($\Delta = 0.33$ ppm) was observed from H_c, suggesting that the proton is the nearest to the neighboring molecules in concentrated solution leading to the highest shielding effect.

The self-association constants (K_a) of each proton was estimated from the experimentally obtained, concentration-dependent NMR spectra for a quantitative comparison.[18] As described above, H_c has the highest K_a of 30.2 L/mol among other protons (Figure 3). This result indicates that spontaneous assembly through $\pi-\pi$ interaction is expected. Nevertheless, the K_a value is still lower than structurally similar pyrazine-containing fused aromatic compounds without *t*-butyl groups,[19] implying that extensive π-aggregation was suppressed by bulky *t*-butyl groups to some extent.

Prior to SA, the crystals of compound **1** formed from a slow evaporation of methylene chloride solution were characterized with XRD to gain insight in the molecular packing. As shown in Figure 4, the XRD pattern obtained from the crystal exhibited well-resolved diffraction patterns including a strong peak at $2\theta \approx 24°$ corresponding to $d \approx 3.7$ Å, which is characteristic of an effective $\pi-\pi$ stacking distance, indicating that the $\pi-\pi$ interaction is one of the driving forces for the formation of the crystal.

SA of **1** was accomplished through a phase transfer method. To varying concentrations of **1** in methylene chloride from 0.1 to 8 mM was very slowly added methanol to maintain two phases. Thereafter, the slow diffusion of the two phases initiated the molecular assembly. In all cases, the volume ratio between methylene chloride, and methanol was kept constant (1:0.8). The morphological study as a function of the concentration was first carried out with SEM. As shown in Figure 5, a clear morphological transformation was observed when the concentration of methylene chloride solution was increased. At 0.1 mM, short and straight strands were found (Figure 5a), whereas at higher concentrations, fibrous structures were formed. Some systems such as perfluoroarene-substituted oligo(*p*-phenylenevinylene) have also shown a morphological change from short to long fibers as the concentration increased.[20] The transition from the straight strands to flexible fibers were clearly observed at the concentration of 0.3 mM by the coexistence of the two distinctively different assembled structures (Figure 5b). From 0.5 to 2 mM, the morphologies revealed entangled flexible nanofibers of approximately 150 nm in width, leading to twisted bundles of fibers as shown in Figure 5c−e. In some cases, extreme coiling of fibers was also observed. SA from more concentrated solutions (above 4 mM) of **1** had a dense packing of flatter fibers with less bundling (Figure 5f and the Supporting Information). It should be noted that SA from concentrations above 4 mM showed partial gel-like behaviors. The morphological transformation from straight strands to nanofibers was further supported by transmission electron microscopy (TEM) and polarized optical microscopy (POM) (see the Supporting Information).

The molecular aggregation of **1** was further evaluated by UV−vis spectroscopy (Figure 6). Compound **1** in chloroform exhibited two λ_{max} at 400 and 421 nm with a broad shoulder

(18) (a) Horman, I.; Dreux, B. *Helv. Chim. Acta* **1984**, *67*, 754–764. (b) Shetty, A. S.; Zhang, J.; Moore, J. S. *J. Am. Chem. Soc.* **1996**, *118*, 1019–1027.

(19) Gao, B.; Wang, M.; Cheng, Y.; Wang, L.; Jing, X.; Wang, F. *J. Am. Chem. Soc.* **2008**, *130*, 8297–8306.

(20) Babu, S. S.; Praveen, V. K.; Prasanthkumar, S.; Ajayaghosh, A. *Chem.—Eur. J.* **2008**, *14*, 9577–9584.

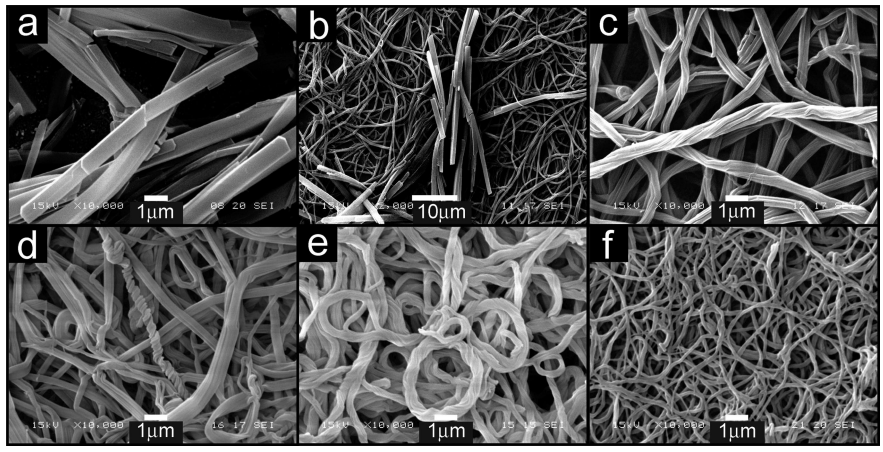

Figure 5. SEM images of assembled structures of **1** obtained from (a) 0.1, (b) 0.3, (c) 0.5, (d) 1, (e) 2, and (f) 8 mM methylene chloride solution.

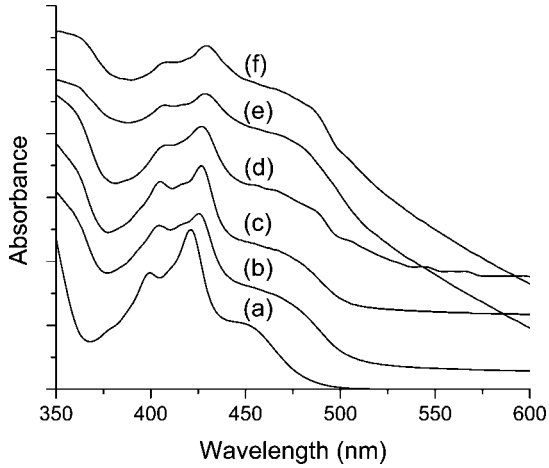

Figure 6. UV−vis absorption spectra of **1**: (a) chloroform solution, (b) methylene chloride/methanol binary solvent, (c) cast film, (d) SA from 0.1 mM methylene chloride solution, (e) SA from 0.5 mM methylene chloride solution, and (f) SA from 1 mM methylene chloride solution.

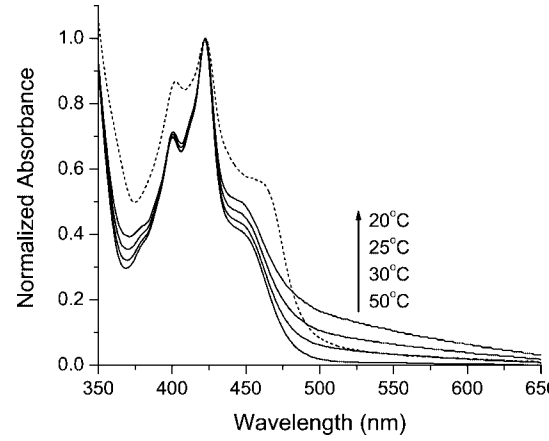

Figure 7. Variable-temperature UV−vis absorption spectra of **1** (dotted line, as-prepared suspension in DMF at 23 °C; solid lines, DMF suspension at 50, 30, 25, and 20 °C, from bottom to top).

around 450 nm which is due to intrinsic molecular properties rather than aggregation confirmed by Beer's law. When a poor solvent (methanol) was added to the methylene chloride solution slowly to decrease the solubility, the peaks at 400 and 421 nm were gradually red-shifted to new λ_{max} at 406 and 426 nm, respectively. In addition, the overall spectrum became much broader with increased absorbance at 450 nm. We also performed UV−vis on a cast film of **1**. The absorption of the cast film of **1** showed almost the same behavior as that in methylene chloride/methanol binary solvent, indicating that the spectral change upon the addition of methanol to the methylene chloride solution was caused by molecular aggregation rather than solvent polarity change. In the case of self-assembled structures from 0.1, 0.5, and 1 mM solutions, the absorptions were similar to that of the cast film with further red-shifted λ_{max} up to 409 and 429 nm with more pronounced absorbance at the shoulder region. The spectral change in the binary solvent, cast film, and self-assembled structures indicates that intermolecular $\pi-\pi$ interactions are involved in the molecular aggregation. For SA from concentrations of 2 mM and beyond, we were unable to conduct UV−vis because thin films of fibers were not obtained.

To confirm that the red-shifted shoulder in the solid state was originated from π-aggregation, we performed a variable-temperature UV−vis experiment (Figure 7). First, a suspension of **1** in *N*,*N*-dimethylformamide (DMF) was prepared by sonication. The absorption of the DMF suspension showed a red-shifted shoulder at ca. 462 nm with increased absorbance compared to that in the chloroform solution. When the suspension was heated to 50 °C, the absorption at the shoulder was blue-shifted to 450 nm with lower absorbance that was identical to the absorption in the solution state. This result verifies that the spectral change in the DMF suspension at room temperature (which was similar to UV−vis in the solid state presented in Figure 6) was due to π-aggregation. The UV−vis recorded upon cooling showed an increase in the absorbance at the shoulder region. It should be noted that the absorption at 20 °C after cooling was different from that of as-prepared DMF suspension. This is due to the fact that the π-aggregates formed from the cooling process are not identical to those in the as-prepared DMF suspension.

XRD measurements were used to investigate molecular packing of assembled structures observed by SEM measurement. The XRD patterns obtained from the assembled structure of **1** induced at various concentrations are shown in Figure 8. As expected, the assembled structures having different morphologies resulted in different XRD patterns. A similar XRD pattern as that of the crystal of **1** with a peak

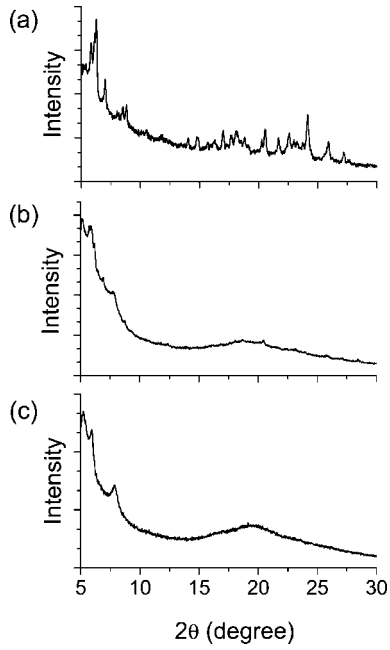

Figure 8. X-ray diffraction patterns of assembled structures of **1** obtained from (a) 0.1, (b) 0.5, and (c) 8 mM methylene chloride solution.

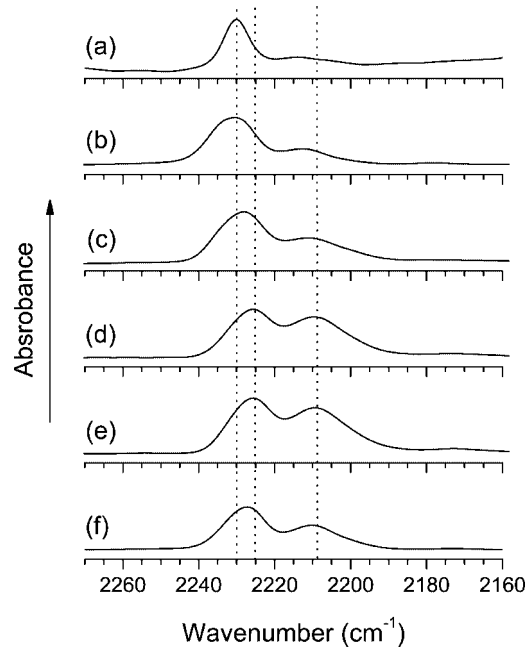

Figure 9. FT-IR spectra in the CN stretching region for (a) solution in CCl_4, and assembled structures obtained from (b) 0.1, (c) 0.5, (d) 1, and (e) 8 mM solution and (f) crystal of **1**. FT-IR mode: (a) transmission, (b) absorption−reflection, (c−f): ATR.

at $2\theta \approx 24°$ corresponding to $\pi-\pi$ stacking distance was observed from short and straight strand assembled from 0.1 mM solution. In contrast, flexible nanofibers obtained from higher concentrations from 0.5 mM to 8 mM showed an amorphous character with a broad peak centered at $2\theta \approx 19°$ corresponding to $d \approx 4.6$ Å, which was frequently observed from well-organized π-conjugated polymers.[21] It is interesting to note that the peak for $\pi-\pi$ stacking distance was not observed.

To explore the role of cyano interactions in the morphological changes, the assembled structures were characterized by ATR or absorption-reflectance FT-IR spectroscopy focusing on cyano stretching region. First, a very dilute solution (1.8×10^{-5} M) in CCl_4 was subjected to transmission FT-IR to identify free cyano stretching. As shown in Figure 9a, free cyano stretching appeared as a single sharp peak at 2230 cm^{-1}. In the case of self-assembled structures, significant changes in the cyano stretching region were noticeable (Figure 9b−e). A broad peak centered at 2230 cm^{-1} and a small peak at 2210 cm^{-1} were observed for the straight strands assembled from 0.1 mM solution. When the concentration was increased to 0.5 mM, the peak at higher frequency was slightly shifted to 2228 cm^{-1} and the frequency of other peak at 2210 cm^{-1} remained unchanged. The peak at 2228 cm^{-1} showed a broad and asymmetrical shape which could be resolved into two different bands at 2230 and 2225 cm^{-1}. FT-IR spectrum of nanofibers assembled from 1 mM showed further shift of the higher-frequency peak to 2225 cm^{-1} while maintaining the other peak at 2210 cm^{-1}. The intensity of the lower frequency peak was gradually increased from 0.1 mM and became almost equal to that of the higher frequency peak at 1 mM. At concentrations higher than 1 mM, the peak at 2210 cm^{-1} was shifted to 2208 cm^{-1}. The FT-IR spectrum of the crystal of **1** obtained from a 10 mM methylene chloride solution also exhibited an asymmetrically shaped peak at 2228 cm^{-1} and a small peak at 2210 cm^{-1} (Figure 9f), implying the existence of cyano interactions.

In summary, the SA of **1** in various concentrations resulted in three different peaks at 2230, 2225, and 2208 cm^{-1}. In light of the FT-IR experiment in CCl_4 solution, we assign the peak at 2230 cm^{-1} as free cyano stretching. For the self-assembled structures, the free cyano peak gradually shifted to 2225 cm^{-1} as the solution concentration increased from 0.1 mM to 1 mM, and no further change was observed at the concentrations above 1 mM. This indicates that the contribution of intermolecular cyano interaction becomes more significant as the solution concentration increases from 0.1 mM to 1 mM. As for the peak at the lower frequency (2208 cm^{-1}), there may be two possible interpretations: (1) additional cyano stretching from different modes of interaction because cyanophenyl can engage in various interaction modes, including CN···HC interaction and CN···CN dimerization,[11,13] which have shown different shifts in frequency;[22] (2) C≡C stretching due to the more asymmetric environment when cyano groups are engaged in intermolecular interactions. Although we are unable to assign the exact origin of the lower frequency peak, it is clear that both possibilities are the result of cyano interaction.

Compound **1** can have three intermolecular interactions; $\pi-\pi$, cyano, and van der Waals. The directions of $\pi-\pi$ and cyano interactions are perpendicular to each other. Presumably, at low concentrations (0.1 mM), straight strands are grown via $\pi-\pi$ interactions, whereas lateral organization is

(21) (a) Chen, S.-A.; Chang, E.-C. *Macromolecules* **1998**, *31*, 4899–4907. (b) Blouin, N.; Michaud, A.; Gendron, D.; Wakim, S.; Blair, E.; Neagu-Plesu, R.; Belletête, M.; Durocher, G.; Tao, Y.; Leclerc, M. *J. Am. Chem. Soc.* **2008**, *130*, 732–742.

(22) Hori, K.; Kuribayashi, M.; Iimuro, M. *Phys. Chem. Chem. Phys.* **2000**, *2*, 2863–2868.

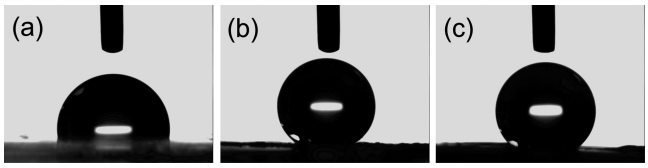

Figure 10. Images of water droplet on surface of (a) spin-coated film and nanofiber films of **1** obtained from (b) 0.5 and (c) 8 mM solution.

facilitated by cyano interactions. In this case, the $\pi-\pi$ interaction between oligo(*p*-phenyleneethynylene)s in compound **1** may play an important role.[7n,o] Meanwhile, the growth of the flexible nanofibers may be driven by cyano interactions, whereas $\pi-\pi$ interactions exist in the lateral direction. However, the $\pi-\pi$ interactions are not as well-defined as in the case of the crystals or microstrands lacking typical diffraction for $\pi-\pi$ stacking distance in XRD. The steric effect of *t*-butyl groups in the T-π-core must influence the formation of nanofibers significantly at high concentrations.

SA at low concentrations or the slow recrystallization process allows for the optimum molecular packing geometry that accommodates the steric *t*-butyl group while maintaining well-defined $\pi-\pi$ stacking. At high concentrations, cyano interactions may grow faster than $\pi-\pi$ interactions because *t*-butyl groups do not interfere with cyano interactions. Such steric effects of bulky *t*-butyl groups on π-aggregation were observed from the concentration-dependent ^{1}H NMR study. The morphological transformation is well-manifested by the coexistence of two different assembly morphologies at 0.3 mM. When the fibers assembled at the transition concentrations (higher than 0.1 mM and lower than 1 mM) were left undisturbed, they rearranged to form straight strands in a few days, indicating that the microstrands are thermodynamic products. However, at concentrations equal to and higher than 1 mM, the morphology of the fibers did not show any time dependence. This result complies with the observation from FT-IR that showed fully developed cyano interactions at 1 mM. At concentrations beyond 4 mM, bundling of small fibers, which was dominant at lower concentrations, was absent. A relatively higher density of small fibers due to higher nucleation and branching produces three-dimensional entanglements while trapping solvent, which prevents further bundling exhibiting partial gel-like behavior at high concentrations.

The surface properties of the film covered with nanofibers were analyzed by WCA measurement. As a reference, a spin-coated film was prepared using methylene chloride solution of **1** on a cover glass substrate. The WCA of spin-coated film was found to be 99° (± 1°) as presented in Figure 10. The value increased significantly to 139° (± 1°) in the case of the film composed of nanofibers assembled from 0.5 mM solution. Interestingly, the WCA remained constant for the nanofibers from concentrations beyond 0.5 mM. For example, WCA of fibers from 8 mM was 140° (± 1°).

Typically, the surface hydrophobicity can be tuned by modifying surface roughness or functional groups.[23] Therefore, an increase in hydrophobicity from spin-coated film to nanofiber film could be attributed to the nanometer scale roughness. In addition, fibers grown along the cyano interaction direction may be decorated by hydrophobic alkyl chain making nanofibers hydrophobic, which supports the mechanism of formation of flexible nanofibers.

Conclusions

We have demonstrated the utility of the cyanophenyl group in T-shaped asymmetric bisphenazine containing a large aromatic core to induce 1D assembly and manipulate assembling morphology. The molecule tends to aggregate in solution through $\pi-\pi$ stacking due to a large and flat aromatic core, which was evident in the concentration-dependent ^{1}H NMR and UV−vis absorption spectra. The SA using the phase transfer method with methylene chloride/methanol binary solvent system showed that assembled morphologies are easily changed from straight strands to nanofiber bundles with substantial coiling and to flat nanofibers with less bundling and coiling as solution concentration increased. The SEM, XRD, and FT-IR analyses were utilized to identify the driving forces for the morphological transformation. Although the XRD patterns for the straight strands exhibited the evidence of $\pi-\pi$ stacking at $d \approx 3.7$ Å, this diffraction was absent for the nanofibers. In addition, the IR spectrum obtained from the strands showed major cyano stretching peak at 2230 cm^{-1}, representative of the free cyano group. However, the IR spectrum for nanofibers suggested intermolecularly interacted cyano groups. As a result, two different intermolecular interactions, $\pi-\pi$ and cyano interaction, competitively induced different assembled structures depending on the solution concentration. The presence of steric *t*-butyl groups in the π-core must have a significant influence in the competition of the two driving forces. In conjunction with our previous report with respect to the cyano group's ability to tune the electronic properties of the T-core,[16] the results of this research demonstrate the unique utilization of the cyano group in regard to molecular assembly by providing a simple and convenient methodology to manipulate the assembly morphology.

Acknowledgment. We are grateful to Dr. Longzhou Ma, from the Harry Reid Center for Environmental Studies at UNLV, for TEM measurements.

Supporting Information Available: Additional SEM, transmission electron microscopy (TEM), and polarized optical microscopy (POM) images of self-assembled structures of **1** (PDF). This material is available free of charge via the Internet at http://pubs.acs.org.

CM8029455

(23) (a) Acatay, K.; Simsek, E.; Ow-Yang, C.; Menceloglu, Y. Z. *Angew. Chem., Int. Ed.* **2004**, *43*, 5210–5213. (b) Singh, A.; Steely, L.; Allcock, H. R. *Langmuir* **2005**, *21*, 11604–11607. (c) Zhou, Y.; Yi, T.; Li, T.; Zhou, Z.; Li, F.; Huang, W.; Huang, C. *Chem. Mater.* **2006**, *18*, 2974–2981. (d) Srinivasan, S.; Praveen, V. K.; Philip, R.; Ajayaghosh, A. *Angew. Chem., Int. Ed.* **2008**, *47*, 5750–5754.